buildings

MDPI

Article

Prediction of Urban Construction Land Carbon Effects (UCLCE) Using BP Neural Network Model: A Case Study of Changxing, Zhejiang Province, China

Qinghua Liao [1], Xiaoping Zhang [2,*], Zixuan Cui [2] and Xunxi Yin [3,*]

[1] School of Architectural Engineering, Tongling University, Tongling 244061, China; 087513@tlu.edu.cn
[2] School of Architecture and Urban Planning, Shandong Jianzhu University, Jinan 250101, China; 24270@sdjzu.edu.cn
[3] Zibo Urban Planning Design Institute Co., Ltd., Zibo 255025, China
* Correspondence: rly8921@163.com (X.Z.); xiezi8826@163.com (X.Y.)

Abstract

Against the backdrop of the intensifying global climate crisis, urban construction land (UCL), as a major source of carbon emissions, faces the severe challenge of balancing emissions reduction and development in its low-carbon transformation. This study is dedicated to filling the theoretical and methodological gap in the refined assessment of urban construction land carbon effects (UCLCE) spatial heterogeneity among regions, and proposes and validates an innovative block-scale prediction framework. To achieve this goal, this study takes the central urban area of Changxing, Zhejiang Province, as the study area and establishes a BP neural network model for predicting UCLCE based on multi-source data such as building energy consumption and built environment elements (BEF). The results demonstrate that the BP neural network model effectively predicts the different types of UCLCE, with an average error rate of 30.10%. (1) The total effect and intensity effect exhibit different trends in the study area, and a carbon effect table for different types of UCL is established. (2) The spatial distribution characteristics of UCLCE reveal a distinct reverse-L pattern (“ ⌟”-shaped layout) with positive spatial correlation (Moran’s I = 0.11, $p < 0.001$). (3) The model’s core practical value lies in enabling forward-looking assessment of carbon effects in urban planning schemes and precise quantification of emissions reduction benefits. Optimization trials on representative blocks achieve up to 25.45% carbon reduction. This study provides theoretical foundations for understanding UCLCE spatial heterogeneity while delivering scientifically grounded tools for diagnosing built environment issues and advancing low-carbon optimization in urban renewal contexts. These contributions carry significant theoretical and practical implications.

Keywords: urban construction land; carbon effects; building energy consumption; built environment elements; BP neural network; Changxing

check for updates

Academic Editor: Chi Yan Tso

Received: 24 May 2025
Revised: 4 June 2025
Accepted: 29 June 2025
Published: 1 July 2025

Citation: Liao, Q.; Zhang, X.; Cui, Z.; Yin, X. Prediction of Urban Construction Land Carbon Effects (UCLCE) Using BP Neural Network Model: A Case Study of Changxing, Zhejiang Province, China. *Buildings* **2025**, *15*, 2312. https://doi.org/10.3390/buildings15132312

Copyright: © 2025 by the authors. Licensee MDPI, Basel, Switzerland. This article is an open access article distributed under the terms and conditions of the Creative Commons Attribution (CC BY) license (https://creativecommons.org/licenses/by/4.0/).

1. Introduction

Urban construction land (UCL) serves not only as the primary spatial carrier for human habitation, leisure, entertainment, and industrial production but also as the main carrier of carbon emissions [1]. Although UCL accounts for only 2.4% of the global land area, it is responsible for approximately 80% of the world’s energy consumption-related carbon emissions [2,3]. Therefore, mitigating the urban construction land carbon effects (UCLCE) is a key component in addressing global climate change and achieving the

country's "dual carbon strategy". The UCLCE is significantly correlated with the built environment elements (BEF) [4]. Low-carbon oriented spatial planning can solidify the form, quantity, and intensity of the UCLCE by adjusting and optimizing BEF, such as land use function, development capacity, and building spatial form. Its "lock-in effect" and "overall planning function" play a crucial leading role in achieving low-carbon urban development [5,6]. Therefore, delving into the influence mechanism of BEF on the UCLCE and quantitatively forecasting the different types of UCLCE through scientific models and data can serve as an objective foundation for precisely evaluating the carbon impacts of planning schemes [7]. Simultaneously, it provides crucial technical support for urban low-carbon emissions reduction decision-making processes, thereby facilitating the formulation of more targeted and effective strategies to mitigate UCLCE [8].

Currently, scholars have conducted a significant number of fruitful studies on the prediction of the UCLCE. According to different spatial scales, the prediction of the UCLCE can be summarized into the following three categories: (1) Time series prediction. The time series prediction method primarily focuses on the overall regional construction land at the macro scale as the research object. By analyzing the time series changes of socio-economic data, a mathematical model is established through curve fitting and parameter estimation to predict the UCLCE in the future [9,10]. For example, Svirejeva-Hopkins et al. calculated the carbon emissions from construction land in eight regions around the world before 2020 based on the time series changes of population density. By establishing a parametric model, the carbon emissions from construction land by 2050 were predicted, and the characteristics and causes of the changes were analyzed [11]. Chang et al. predicted the peak carbon emissions in 2030 after calculating the UCLCE in China for consecutive years using methods such as the Kaya identity and regression fitting [12]. Yang et al. calculated the UCLCE in the Beijing-Tianjin-Hebei urban agglomeration between 2000 and 2020 and used the Markov model to predict the UCLCE in 2035 [13].

(2) Proxy parameter space allocation. The proxy parameter space allocation method conducts spatial allocation by establishing the quantitative relationship between parameters such as building area, GDP, and population density, and carbon emissions within the town. It then predicts the different types of UCLCE. For example, Chuai et al. utilized proxy parameters such as residential community data and industrial site data for carbon emissions spatial allocation, establishing a 300 $\times$ 300 m carbon emissions prediction grid for major types of construction land, such as residential land, industrial land, and transportation land in the urban area of Nanjing City [14]. Lin et al. used building area data and population density data as surrogate parameters to predict the 200 $\times$ 200 m high spatial resolution carbon emissions distribution map of residential land in two urban areas in southern Taiwan [15]. Based on the proxy parameter space allocation method, Zhang et al. compared the potential of POI data and NPP-VIIRS data for modeling different types of carbon emissions in China. They used POI data to establish spatial grids of different scales to analyze the spatial structure of carbon emissions in different cities such as Beijing, Lanzhou, and Shanghai [16].

(3) Dynamic energy consumption simulation. Dynamic energy consumption simulation methods collect information on the functions of buildings, their envelope structures, wall materials, etc., and predict the carbon effects caused by building energy consumption on UCL based on various simulation software. Commonly used software includes EnergyPlus (23.2.0), DesignBuilder (v7), VirVil-HTB2, etc. For example, Al-Kabaha et al. used EnergyPlus software to integrate the geometric control module of individual building forms in residential areas and the microclimate analysis module, among others, to simulate the building energy consumption of typical residential areas. Results indicated that optimizing these parameters could save about 21.26 GJ (43.63%) in energy usage and

1143.31 kg (43.65%) in emissions [17]. Eid et al. used EnergyPlus software to simulate the impact of these interactions on the energy and carbon emissions of a medium-sized supermarket in Paris [18]. Bahadori et al. used DesignBuilder simulation software to evaluate various energy-saving measures for the heating, ventilation, air conditioning, and lighting systems of a 4-story building in subtropical (hot and humid climate) Central Queensland, Australia [19].

With the rise and continuous development of Artificial Intelligence technology, coupled with its excellent data analysis and prediction performance, some scholars have begun to apply machine learning technology to the prediction of building energy consumption. However, most applications are at the individual building level, and their use in urban—scale planning is more limited. The most used Machine learning prediction methods include BP Neural Network, Support Vector Machine (SVM), and Ordinary Least Square (OLS). However, in specific applications, BP neural networks see the most extensive use in terms of both depth and breadth. Studies show that BP neural networks deliver high prediction accuracy for large datasets and also perform well with small datasets [20]. For instance, Lei et al. developed a prediction model for high-rise building lighting energy consumption by integrating parameters such as lighting energy use, average hourly outdoor temperature, and relative humidity, thereby forecasting air conditioning, electricity, and special energy consumption [21]. Similarly, Zhang et al. conducted a comparative study of indoor environments between earth brick and fired brick buildings in a desert climate, finding that earth brick buildings exhibit superior thermal performance [22]. In terms of energy consumption, Li et al. noted that buildings with thick earth walls consume less energy than typical rural structures [23].

Scholars have made certain progress in the prediction of the UCLCE, but there is still a large knowledge gap regarding how and to what extent the BEF affects the UCLCE, and whether the UCLCE can be scientifically predicted. This study has contributed to this. Firstly, prior studies often focus on individual buildings or single types of construction land, with limited systematic research on urban space UCLCE. Secondly, current prediction methods often allocate results by grid cells of varying precision but overlook the complex plot divisions within construction land, making it difficult to align prediction results with spatial planning land types and boundaries. Thirdly, while BP neural networks are well-established in individual building energy consumption assessment, more empirical research is needed for urban-scale UCLCE prediction.

Against this backdrop, this study focuses on different types of UCL, using controllable BEF from urban and rural planning as input variables and UCLCE as the output variable. A BP neural network prediction model is developed and applied to the planning of Changxing's central urban area in Zhejiang Province, China, offering insights for future low-carbon planning. The study's main contributions are threefold. Firstly, by analyzing the carbon effects of different UCL types, this study proposes UCLCE measurement methods, providing technical support and guidance for urban-scale low-carbon optimization and spatial planning prediction. Secondly, this study introduces a UCLCE numerical table and spatial distribution map at the block level, incorporating land use types and boundaries. These results not only advance high-resolution carbon emissions simulation research but also assist governments in formulating differentiated carbon reduction strategies and support low-carbon and healthy city planning. Thirdly, this study establishes a block-scale predictive framework for regional UCLCE spatial heterogeneity comparison and develops a BEF-based BP neural network UCLCE prediction method. Applied to Changxing's Taihu New Town control planning and urban design, this method clarifies its practical role and application scenarios, offering scientific guidance for low-carbon urban planning and carbon reduction strategy development. This study begins by emphasizing in the Section 1

the theoretical value, practical contribution, and knowledge gap in the literature. The Section 2 explains the study area, research data, and methods. The Section 3 divides the results into three parts: the numerical table of UCLCE based on the block-level, the spatial distribution of the UCLCE, and the spatial autocorrelation of the UCLCE. The Section 4 further discusses the applications, limitations, and further improvements of the results. The Section 5 presents the conclusions.

2. Materials and Methods

2.1. Study Area

Changxing (30°43′–31°11′ N, 116°43′–118°04′ E) is located in Zhejiang Province, China. By the end of 2024, the total area of Changxing was 1430 km^2, with a permanent resident population of 688,000, and it governed 4 sub-districts, 9 towns, and 2 townships. The study area covers the central urban area of Changxing, including four sub-districts, namely Zhicheng Sub-district, Taihu Sub-district, Longshan Sub-district, and Huaxi Sub-district. The urban construction land area is 40.38 km^2, covering different types of UCL, and has diverse BEF characteristics. Additionally, according to the "Overall Planning of Changxing (2017–2035)", the 4 sub-districts within the study area are divided into 933 blocks, including 12 types of lands: village residential land (VRL), urban residential land (URL), industrial storage land (ISL), Business office land (BOL), Cultural and sports land (CSL), Medical land (ML), Commercial land (CL), Hotel land (HL), Science and education land (SEL), Administrative office land (AOL), Green space land (GSL), and Other land (OL).

In recent years, Changxing has experienced high carbon emissions and urgently requires a low-carbon transformation. Firstly, the increasing urban population has led to greater demands for housing, employment, travel, and entertainment, resulting in rapid growth in URL, BOL, ISL, and GSL. According to the "Overall Planning of Changxing (2017–2035)", the study area's population is projected to reach 600,000, and the urban area is expected to expand to 75 km^2 by 2035, nearly doubling its current size. This indicates that the study area will continue to expand for a relatively long time, with carbon control challenges remaining severe. Secondly, Changxing is located in a hot-summer and cold-winter climate zone, which lacks centralized heating infrastructure. Therefore, air conditioning is essential for both heating during winter and cooling during summer, leading to significant building energy consumption. This also increases the sensitivity of the relationship between BEF and UCLCE. Thirdly, Changxing is a typical industrial city, with the secondary industry constituting a high proportion of its economy. In recent years, Changxing has been transitioning to a low-carbon city model, achieving notable success in its economic development strategy.

Given these factors, selecting Changxing as the study area for research on UCLCE prediction is both representative and strategically significant for supporting its low-carbon transformation and development (Figure 1).

2.2. Research Data

Data were collated from two sources. Firstly, based on the classification of building functions in the "Building Energy Consumption Standard (2016)", log in to the marketing system of the power supply company, taking the transformer box as the basic unit, and obtain the electricity consumption data of different locations, times and combinations of positive active power attributes. After screening, 289 different types of construction land blocks were selected as samples. Additionally, energy consumption data of hospitals, schools, and large-scale enterprises within the jurisdiction of Changxing were also collected for verification. Secondly, BEF data on 933 blocks were collected from the Land use map of Changxing. The data were categorized into 4 types: land use, buildings, road systems,

and population. Thirdly, the point of interest (POI) data of all industrial enterprises in Changxing were obtained, including enterprise longitude and latitude information, address name, enterprise name, and enterprise type. It should be noted that after obtaining the original POI data, due to the possible overlap in certain types, such as some enterprise data points existing in both retail business and corporate enterprises, the obtained data needs to be reclassified. Moreover, since web crawler technology cannot accurately identify invalid companies and enterprises when capturing data, it is necessary to manually eliminate the data outside the industrial land according to the distribution of industrial land in the classification of urban construction land in Changxing, and spatially locate the remaining data. Additionally, the POI data obtained on the Baidu Maps website belongs to the Martian coordinate system and has a certain spatial position offset relative to the actual position. Therefore, it is necessary to convert the POI data that has been located and completed into the WGS-2000 coordinate system to form the data that conforms to this study, and conduct visual analysis using ArcGIS (10.2) (Table 1).

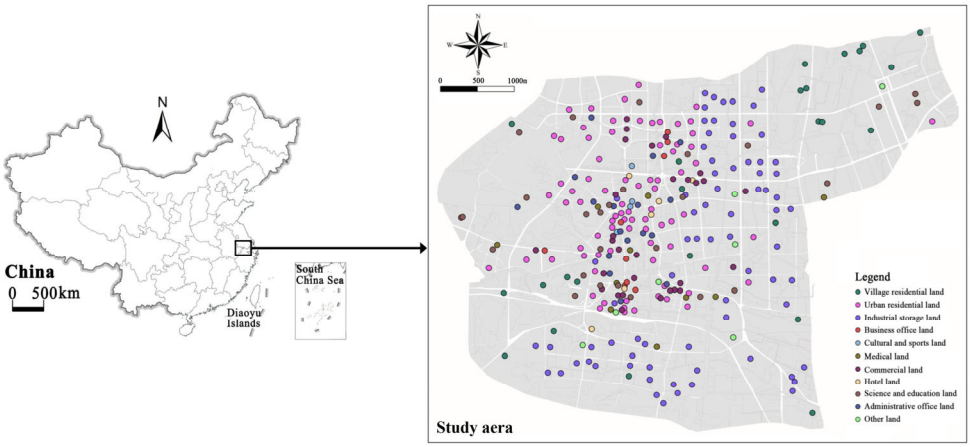


Figure 1. Location of the study area.

Table 1. Data sources and description.

Name	Description	Sources
Industrial POI data	Industrial storage land patch spatial location dataset	Baidu map
Road systems of Changxing	Vector data of road traffic system	Department of Transportation
Land use map of Changxing	Vector map of different land use types	Natural Resources Bureau
Urban population data	Population of urban residential lands	Public Security Bureau
Rural population data	Population of rural residential lands	Public Security Bureau
Architecture data	Building outline contains name, number, height, area, perimeter, and floor information	Construction Bureau
Electricity consumption data	Electricity consumption of Changxing	Statistics Bureau

2.3. Methods

2.3.1. UCLCE Measurement Methods

Carbon emissions from building energy consumption primarily stem from energy use in building operations, including heating, cooling, and lighting. Embodied carbon is embedded in the production, transport, and construction of building materials. From a life-cycle viewpoint, carbon emissions from UCL occur mainly during the building's use phase and represent the "visible" carbon emissions. In contrast, embodied carbon is not generated directly during this phase but constitutes an indirect part of UCLCE. It is not produced on the UCL itself and has a limited connection with the BEF. Moreover, compared to operational energy consumption-related carbon emissions, it accounts for a relatively small proportion. Thus, this study defines UCLCE as the annual carbon emissions from building energy consumption on UCLCE. Specifically, it is divided into three main land types: residential land, industrial and storage land, and public land.

(1) Residential land and public land carbon effects measurement method

The measurement methods of carbon effects for residential land and public land are similar, mainly based on the carbon effect of annual electricity consumption of buildings on the land. The calculation formula is shown in Equation (1).

$$E = AD \times EF \tag{1}$$

where E is the carbon effect of the block (kg); AD represents the electricity consumption. EF is the emissions factor. In this study, the local electricity carbon emissions factor of Changxing is adopted, with a value of 0.8463 $kgCO_2/kwh$.

(2) Industrial and storage land carbon effects measurement method

The measurement methods of carbon effects of industrial and storage land mainly include carbon emissions from enterprise energy consumption and energy consumption in the industrial production process. The calculation formula is shown in Equation (2).

$$C = E_B + E_P \tag{2}$$

where E_B represents the carbon emissions of enterprise energy consumption. The specific calculation method refers to Equation (1). E_P represents the carbon emissions of energy consumption in the industrial production process. The industrial enterprises in the study area do not have energy consumption or carbon emissions during the industrial production process. The relevant enterprises are mainly distributed in other towns and townships within Changxing.

2.3.2. BEF Measurement Methods

The study selected 13 BEFs closely related to the UCLCE from 4 aspects: scale, density, morphology, and land. The calculation formulas for different BEF are shown in Table 2.

Table 2. BEF Measurement Methods.

Type	BEF	Formula	Description	Source
Scale	Building area (BA)	$F = \sum_{i=1}^{n} s_i h_i$ (i = 1, 2, . . ., n)	s_i is the building base area of the i-th building, m^2; h_i is the number of floors of the i-th building; n represents the number of buildings on the block	[24]
	Land area (LA)	$A = S_i$ (i = 1, 2, . . ., n)	S_i is the area of the land of Type i, which is automatically extracted in GIS	[8]

Table 2. *Cont.*

Type	BEF	Formula	Description	Source
Density	Population density (PD)	$P = \frac{M}{S}$	M is the number of people accommodated on the block; S is the land area	[6,25]
	Building density (BD)	$S = \sum_{i=1}^{n} \frac{s_i}{s} (i = 1, 2, \ldots n)$	s_i is the base area of the i-th building on the land. s is the land area; n represents the number of buildings on the block	[26]
	Road network density (RND)	$R = \sum_{i=1}^{n} \frac{L_i}{s}$ $(i = 1, 2, \ldots n)$	L_i is the length of the i-th section of the road within a 1000 m range of the land. s represents the area within a 1000 m range of the land. n represents the number of road sections	[27]
	Green space ratio (GSR)	$Q = \frac{A_i}{S_i}$ $(i = 1, 2, \ldots, n)$	A_i is the green space area of the i-th block; S_i is the area of the i-th block	[28,29]
Morphology	Spatial Compactness (SC)	$K = 2\sqrt{\frac{\pi \times S}{L}}$	S represents the area of the land use; L is the perimeter of the land use	[30]
	Shape factor (SF)	$T = \frac{\sum_{i=1}^{m}(2nh(b+l)+s)}{\sum_{i=1}^{m} nhs}$ $(i = 1, 2, \ldots, m)$	m represents the number of buildings on the block. i is the i-th building; n represents the number of building floors; h represents the floor height of the building; b is the width of the bottom surface of the building; l is the length of the bottom surface of the building; s represents the floor area of the building	[31]
	Building storey (BS)	$H = \frac{F}{\sum_{i=1}^{n} s_i}$ $(i = 1, 2, \ldots, n)$	F is the building area on the block; s_i is the base area of the i-th building on the land. n represents the number of buildings on the block	[32]
	Land orientation (LO)	$X = \frac{A_i}{L_i}$ $(i = 1, 2, \ldots, n)$	A_i is the southbound length of the i-th block; L_i is the perimeter of the i-th block	[33]
Land	Land use (LU)	$G = B_i$ $(i = 1, 2, \ldots, 11)$	B_i is the function of block i. 1 is VRL. 2 is URL. 3 is ISL. 4 is BOL. 5 is CSL. 6 is ML. 7 is CL. 8 is HL. 9 is SEL. 10 is AOL. 11 is OL.	[34]
	Land use mixing degree (LUMD)	$L = \frac{-\sum(A_j ln A_j)}{ln N_j}$ $(j = 1, 2, \ldots, n)$	A_{ij} is the proportion of the area of Class i land within a 1000 m range of the land use. N_j represents the quantity of building land types within a 1000 m range of the land	[35]
	Green space area proportion (GSAP)	$E = \sum_{i=1}^{n} \frac{s_i}{s}$ $(i = 1, 2, \ldots, n)$	s_i is the area of the i-th green space within a 1000 m range of the land use. s represents the area within a 1000 m range of the land. n represents the number of green space	[36]

2.3.3. BP Neural Network Model

The problems solved by machine learning models mainly fall into two categories: classification and prediction. According to existing research, there are relatively many machine learning models used to solve classification problems, including decision trees, random forests, Naive Bayes, etc. Since this study does not cover them, they will not be

elaborated in detail. Among the machine learning prediction models, the Ordinary Least Squares regression, BP neural network, and Support Vector Machine are the most widely used. This study mainly selects the above three models for comparison. Generally, the Ordinary Least Squares regression is well-suited for linear prediction but exhibits poor applicability for nonlinear problems. While Support Vector Machines offer better nonlinear mapping capabilities, they suffer from disadvantages such as slow convergence speed, unstable prediction results, a tendency to fall into local minima during training, and excessive reliance on empirically determined parameters during network construction. This reliance compromises generalization ability. Conversely, the BP neural network possesses strong function approximation capabilities. For predicting UCLCE, where a highly nonlinear relationship exists between inputs and outputs, the BP neural network effectively uncovers underlying patterns. It accurately establishes predictive models, demonstrating superior prediction performance, generalization ability, and stability compared to both Ordinary Least Squares regression and Support Vector Machine. Additionally, the BP neural network has strong self-learning capabilities. It does not require a large amount of sample data to establish a specific mathematical function relationship between UCLCE and BEF. Instead, it can learn from a small amount of sample data to build a mapping relationship, enabling accurate predictions of UCLCE based on the BEF. This makes the BP Neural Network model highly applicable. Scholars have predicted the UCLCE in Chengdu, Shandong, and Zhejiang based on the BP neural network. Therefore, this study employs the BP neural network to predict different types of UCLCE. The prediction results are compared against those from Support Vector Machine, Ordinary Least Squares regression, and multiple linear regression models to verify their reliability (Figure 2).

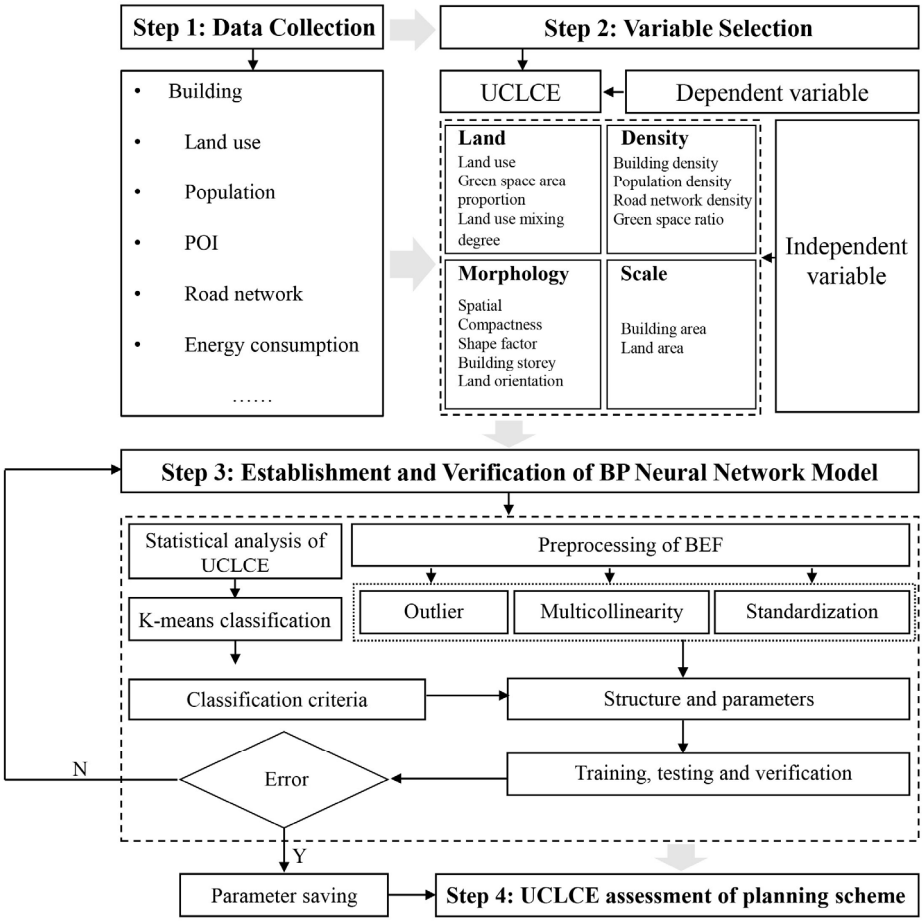


Figure 2. The establishment process of the UCLCE prediction model.

Data processing. The acquisition of knowledge in BP neural networks is mainly obtained from sample data. Therefore, preprocessing the sample data before the BP neural network starts learning can significantly improve the prediction accuracy of the BP neural network. In this study, data preprocessing mainly includes two steps: The first is outlier processing. Because the energy consumption of building operation is affected by various factors, the collected building energy consumption data may contain some "noise", and these data that are prone to cause errors need to be deleted before prediction. The second is standardized processing. The common methods of sample data standardization processing include: min-max normalization, log function conversion, z-score normalization, etc. To ensure the nature of the data and the relative relationship between the data, while compressing the scale of the variables and eliminating the influence of factors with excessive variance on the BP neural network method, the data standardization processing method in this study mainly adopts the ln function transformation method on the basis of eliminating outliers.

Parameter setting. The determination of the structure and related parameters of the BP neural network has a significant impact on the prediction accuracy. In the structure of the BP neural network, both the input layer and the output layer have only one layer, which can be determined relatively easily according to the actual situation. However, the hidden layer can be one or more layers, and it is necessary to reasonably determine the number of layers of the hidden layer, the number of neurons in different layers, and other related parameters. Studies show that the BP neural network with a single hidden layer is more suitable for small sample prediction due to its simple structure and the ability to map any dimension of space. Therefore, the number of hidden layers in this study is determined to be 1. The determination of the number of neurons in the hidden layer is mostly based on referring to the following empirical formula and comprehensively determined through continuous experiments Equation (3).

$$m = \sqrt{n + l} + \alpha \tag{3}$$

where m is the number of neurons in the hidden layer, n is the number of neurons in the input layer, l is the number of neurons in the output layer, and α is a constant between 1 and 10.

After determining the structure of the BP neural network, the determination of other related parameters such as the maximum number of training sessions, learning rate, and momentum factor, is also very important. The purpose of setting the above related parameters is to quickly meet the prediction accuracy requirements after multiple trainings. In contrast, relevant parameters such as the maximum number of training sessions, learning rate, and momentum factor are relatively fixed, and only their initial values need to be determined. However, it should be noted that the determination of the initial values is affected by various factors, such as the size of the training data, the selection of input variables, and the structure of the BP neural network (Table 3).

Average error rate verification. BP neural network model is a multi-layer feedforward neural network based on the error reverse propagation algorithm. There are three or more layers of structure, namely the input layer, the hidden layer, and the output layer. Each layer is composed of several neurons. The neurons between each layer are fully connected, while the neurons within each layer are not connected. The output value on each neuron is determined by the input value, the Sigmoid excitation function, and the threshold. In this study, the toolbox built into the MATLAB (R2024b) platform was utilized. By inputting the running code in the editor tool, parameters such as the number of neurons in the input layer, output layer, and hidden layer were determined to achieve the construction and verification of the BP neural network model. Meanwhile, to verify the reliability of the

model, the average error rate is adopted to calculate the Loss value, which is represented by R. The calculation formula is shown in Equation (4).

$$R = \frac{1}{n}\sum_{i=1}^{n}\left|\frac{Y_i - \overline{Y}_i}{Y_i}\right| \quad (4)$$

where n represents the number of test samples; Y_i is the true value of the i-th sample; $\overline{Y}_i$ is the predicted value of the i-th sample. The closer the value of R is to 0, the higher the accuracy of the prediction.

Table 3. Training parameters of BP neural network.

Parameters	Value
net. trainParam. epochs	10,000
net. trainParam. goal	0.001
net. trainParam. lr	0.8
net. trainParam. mc	0.6
net. trainParam. max_fail	10,000
net. trainParam. mem_reduc	3
net. trainParam. show	100

Comparative verification. Due to the large number of types of UCL, the UCLCE differences of some types are not significant. If they are directly statistically analyzed and predicted, it will lead to a relatively low confidence level of the results. Therefore, first of all, the K-means model in machine learning is studied to conduct unsupervised clustering of the current construction land according to carbon emissions. Therefore, the study first adopts the K-means model in machine learning to conduct unsupervised clustering of the UCL according to carbon effects. Based on the clustering results, this study unfolds respectively according to the seven more distinct classifications of residential land (RL), ISL, administrative land (AL), SEL, CL, ML, and OL. Secondly, based on the clustering results, after being tested by the multicollinearity analysis method, the BP neural network model trained based on the full sample is used to predict the remaining classified blocks and planning schemes. For missing values, they are processed according to the average value of the samples of this type. Finally, by comparing with other methods, the scientific and reliability of the conclusion are further verified. Based on the selected BEF, a training network model for the UCLCE was established. About 10% of the sample data was randomly selected to test the training network model and verify the accuracy of the model. After multiple trainings, the results show that the average error rate of the model is 30.10% (Figure 3). This error level is somewhat reasonable compared with the current related studies. In many similar studies, especially in prediction models involving complex systems and multi-source data, the prediction error is usually between 20–40%. For example, Luo et al. established a carbon emission prediction model based on building energy consumption data, with an average error of approximately 26.05% [37]. Lee et al. found in a similar study that the errors of the carbon emissions prediction models for summer and winter were 37.73% and 38.57% respectively [38].

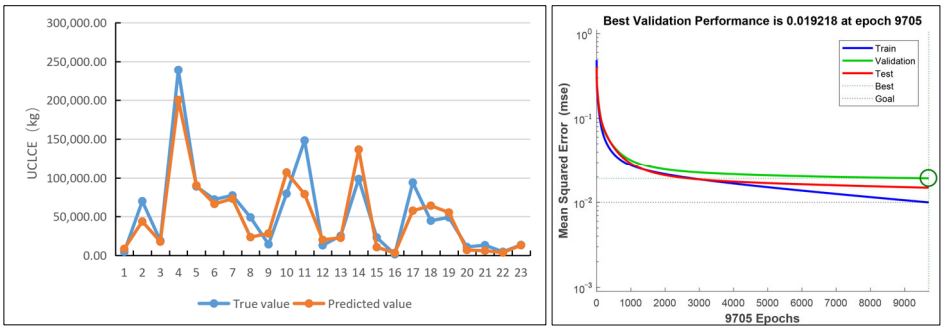


Figure 3. Validation of UCLCE prediction model.

This error range is mainly attributed to the following aspects: Firstly, the UCLCE at the block scale is influenced by a variety of complex factors, including building types, energy usage patterns, population density, etc. The dynamics and uncertainties of these factors increase the difficulty of prediction. Secondly, during the integration and processing of multi-source data, there may be certain information loss or inconsistency, which will also affect the prediction accuracy of the model. Finally, the number of samples of different types, as well as the training process and parameter settings of the BP neural network model, will also have an impact on the prediction results. Nevertheless, the model of this study can still capture the main trends and spatial distribution characteristics when predicting the carbon effects of different types of construction land, and its prediction results have important reference value for low-carbon urban planning. Therefore, by saving the optimal training parameters, the different types of UCLCE are predicted.

Additionally, the sample data of URLs were selected to establish the BP neural network prediction model, the Ordinary Least Square regression, and the Support Vector Machine, respectively, and the best prediction model was determined by comparing with the true values. After multiple calculation results, it is found that for URL, the prediction error rate of the BP neural network model is 11.22%, the prediction error rate of the Support Vector Machine is always less than 1%, and there is a risk of overfitting caused by insufficient sample size. The prediction error rate of the Ordinary Least Square regression model is 35.02%. When predicting the UCLCE from the perspective of building energy consumption, the BP neural network is the best. By comparing the prediction model with multiple linear regression and substituted parameter space allocation methods, it is found that the adjusted R^2 of multiple linear regression is less than 0.2, while the results of substituted parameter space allocation fail to provide clear geographical locations and boundaries for land use carbon effects.

2.3.4. Spatial Autocorrelation of UCLCE

Spatial autocorrelation analysis is a method to judge the degree of correlation between two or more variables through the analysis of correlation, which is divided into Global Moran's I and Local Moran's I [39]. In this study, local Moran's I was selected for correlation analysis [40]. Firstly, the local Moran's I can identify the correlation between typical and atypical regions, such as "hot spots" and "cold spots", by analyzing the correlation between the observed values and the values of neighboring points in the test space [41]. Secondly, using LISA clustering in the spatial econometric software Geoda (V 1.20) and drawing on the theory of life circles, three spatial weight matrices were constructed for distances of 500 m, 1000 m, and 1500 m, respectively. Based on the spatial weight matrix of three distances, the Moran'I was calculated, and the clustering characteristics of the UCLCE were analyzed, and it was divided into four types: "High-High" cluster, "High-Low" cluster, "Low-Low" cluster, and "Low-High" cluster. Then, the spatial distribution law is analyzed [42].

The value of Moran's I is distributed between [−1, 1]. Moran's I is greater than 0, indicating a positive correlation [43]. The closer the value is to 1, the stronger the agglomeration degree is. Moran's I is less than 0, indicating a negative correlation. The closer it is to −1, the greater the difference [43]. The calculation formula is shown in Equation (5).

$$I = \frac{n\sum_{i=1}^{n}\sum_{j=1}^{n} w_{ij}(x_i - \overline{x})}{\sum_{i=1}^{n}\sum_{j=1}^{n} w_{ij}(x_i - \overline{x})^2} \quad (5)$$

where n represents the total number of land patches within the study area, w_{ij} is the spatial weight, x_i is the variable observed in patch i, x_j is the variable observed in patch j, $\overline{x}$ is the mean of the observed value.

3. Results

3.1. Numerical Table of UCLCE

Based on the prediction results of the BP neural network, the current numerical table of different types of UCLCE in the central urban area of Changxing was obtained, including the total effect and intensity effect (Table 4). The total effect shows ISL–OL–ML–RL–SEL–CL–AL. The intensity effect shows a decreasing trend of ISL–ML–CL–OL–RL–AL–SEL. Based on the numerical table, it not only helps to clarify the types of construction land with high carbon effects in cities, thereby guiding low-carbon urban renewal, but also can assist in the comparison and selection of multiple schemes under the low-carbon goal.

Table 4. Different types of total effect and intensity effect.

Type	Mean Total Effect ($kgCO_2/m^2$)	Mean Intensity Effect ($kgCO_2/m^2$)
RL	760,601.25	12.76
ISL	6,346,118.38	86.99
AL	175,911.9	12.40
SEL	586,458.01	8.43
ML	1,201,185.03	65.99
CL	554,470.07	28.93
OL	2,011,613.45	16.87

This study converts UCLCE into building area-based energy consumption intensity, and compares it with the "China Building Energy Efficiency Development Report (2018)", the "Energy Consumption Standard for Civil Buildings (2016)", and other scholars' work. The energy consumption intensity per unit building area for residential and administrative office buildings aligns with these references, falling within 10–20.00 kWh/m^2. Other scholars' findings vary and are used for reference only. For building types like cultural venues, sports facilities, medical buildings, and commercial buildings, the energy consumption intensity per unit building area is slightly lower. The disparity mainly arises because our field research data is heavily influenced by vacancy rates. In field research, we observed that some newly built shopping malls or office buildings have high vacancy rates and low levels of human activity, which significantly reduces UCLCE below the ideal or reference values in relevant studies. Nevertheless, comparisons with typical, mature blocks in Changxing's central urban area show alignment. For example, Yaohan Shopping Mall's energy consumption intensity per unit building area is 169.29 kwh/m^2, and Changxing People's Hospital's is 109.54 kwh/m^2, both of which match existing research.

3.2. Spatial Distribution of UCLCE

Based on the prediction results of the UCLCE by BP neural network, the carbon effect vector map is obtained. It can be seen that the different types of UCLCE in the central urban area of Changxing present the following characteristics in space. (1) "⌟" spatial layout pattern (Figure 4). On one hand, the high-carbon effect areas mainly correspond to the Economic Development Zone of Changxing. According to the UCLCE numerical table, it can be known that the total effect and intensity effect of ISL are both higher than those of other types of UCL. On the other hand, when excluding undeveloped land, the areas with low-carbon effects primarily correspond to Changxing's old city core. These areas are predominantly characterized by low-carbon land types, including RL, CL, and AL. The building and land areas within these districts are relatively compact. In contrast, the RND and LUMD metrics are comparatively high.

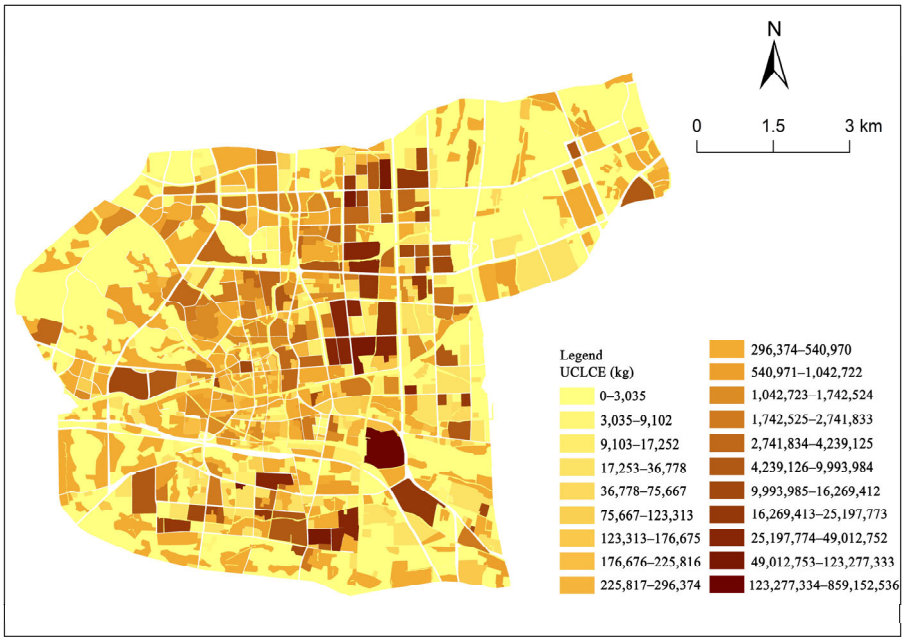


Figure 4. Spatial distribution characteristics of UCLCE.

(2) Spatial positive correlation. The spatial distribution characteristics of the UCLCE were further analyzed by using the spatial autocorrelation method. The global spatial autocorrelation Moran's I calculated by GeoDa software was 0.11, and the *p*-value was 0.001, exceeding the confidence level of 99.9%. This indicates that the UCLCE in the central urban area of Changxing is not randomly distributed but shows a significant spatial positive correlation, further revealing the spatial agglomeration pattern of the UCLCE (Figure 5). On one hand, Moran's I value is used to measure the correlation of the research object in spatial distribution. The value range is usually between −1 and 1. A positive value indicates a positive spatial correlation, that is, the carbon effects of adjacent blocks are mostly distributed within the same interval range. In this study, Moran's I value was 0.11, which was at a relatively low level. However, it was highly significant at the $p < 0.001$ level. This low but significant spatial positive correlation implies that in urban planning and the formulation of carbon emission reduction strategies, attention should be paid to the spatial correlation between different regions, taking into account the mutual influence of carbon effects in adjacent regions. On the other hand, this study reveals that the UCLCE in the study area has a non-negligible micro-scale spatial dependence structure and a certain degree of spatial aggregation. Specifically, the UCLCE is not completely randomly distributed in space. Regions with similar carbon effects show certain aggregation characteristics,

presenting a spatial distribution feature where carbon emissions hotspots are distributed in small-scale clusters, and the spatial isolation effect of carbon blocks on high-carbon blocks is significant. For instance, in areas dominated by CL development and featuring a high density of transport facilities, the surrounding blocks exhibit similar functional attributes and levels of human activity intensity. As a result, the carbon effect tends to cluster at a comparable level. This spatial agglomeration model is of crucial guiding significance for the subsequent formulation of targeted carbon emissions reduction strategies and the optimization of urban spatial layout.

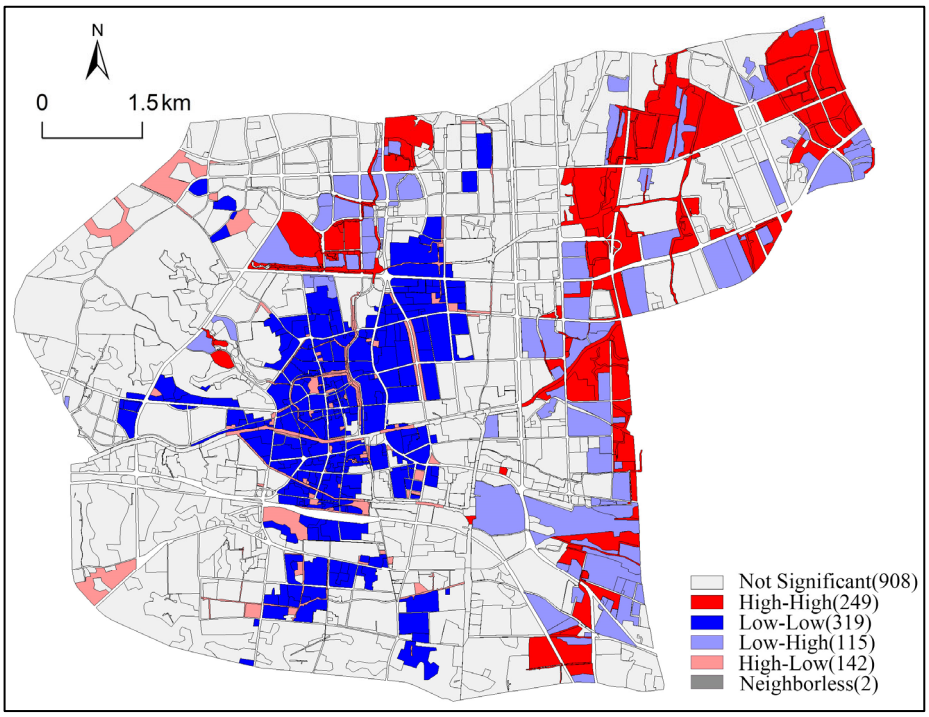


Figure 5. Spatial Agglomeration Characteristics of UCLCE.

3.3. Spatial Distribution of BEF

Through the measurement and visualization analysis of different types of BEF in ArcGIS, we can systematically reveal the spatial distribution characteristics and interrelationships of various BEF. On one hand, through the precise measurement of different types of BEF, the basic characteristics such as the quantity, density, and coverage of each type of BEF can be comprehensively grasped, thereby obtaining the numerical range table of different types of BEF. On the other hand, combined with the powerful spatial analysis function of ArcGIS, a series of intuitive visual maps can be generated to clarify the spatial distribution pattern of the BEF and reveal their unique and diverse distribution characteristics, thereby providing important data support and decision-making references for urban planning and management (Figure 6). For example, the land types with relatively high BD in the study area are mainly ISL and CL, which are distributed in the east and south of the core area. Among them, CLs are mainly concentrated in the city center or near transportation hubs, forming high-density commercial clusters. Meanwhile, the volume of commercial buildings such as commercial complexes is relatively large, which leads to a high BD. ISLs are mainly distributed on the urban edge or along major traffic arteries, presenting a band-like or clustered distribution. Moreover, due to the need to meet the production demands of enterprises, the building dimensions of ISL are generally large, resulting in a high BD. Therefore, it can provide a scientific basis for further exploring the

underlying socio-economic motivations and urban planning logic, and for the optimization and sustainable development of urban space.

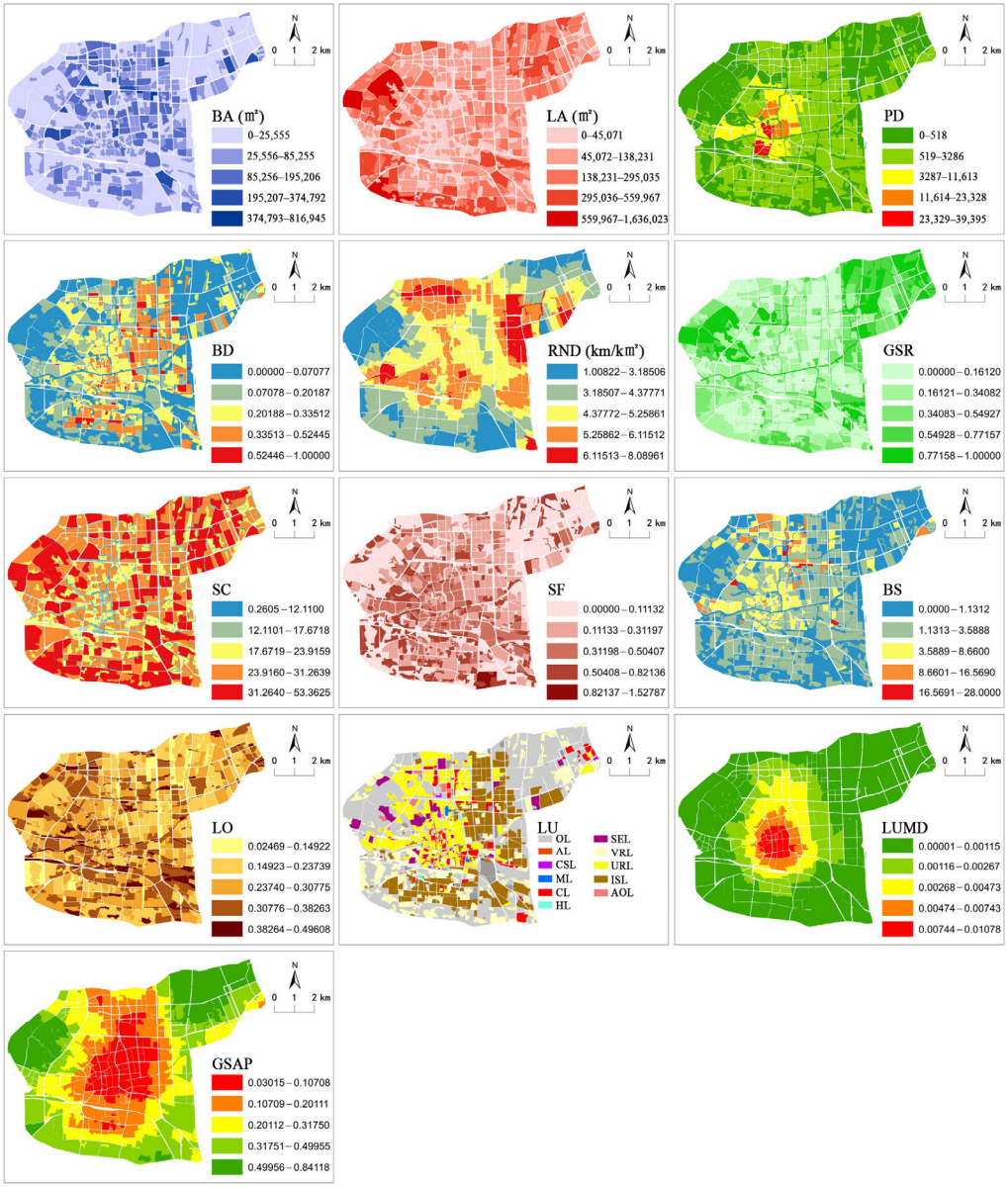


Figure 6. Spatial Distribution of BEF.

4. Discussions

4.1. Influence Mechanism

4.1.1. UCL: The Spatial Carrier of Carbon Effects

Understanding the connotation of the UCLCE is a prerequisite for making predictions [44]. The "carbon effect" is developed from the concept of "effect", mainly referring to the impact brought about by the increase or decrease of carbon emissions [45]. The UCLCE refers to the material and energy flow and their interaction, adaptation between the BEF and carbon emissions, and carbon absorption processes at a certain spatial scale. The UCLCE refers to the interaction between material-energy flows and carbon processes.

By optimizing the BEF of different types of UCL to enable them to have the ability to cope with the increase or decrease in carbon emissions, the goal of carbon reduction can be achieved. Studies show that the UCLCE can be positive or negative, and the carbon effects of different types of UCL exhibit significant spatial differentiation and intensity

differences [46,47]. This study mainly focuses on carbon source land, specifically including RL, CL, and ISL, etc. The carbon effects of these UCL show a positive effect. In contrast, ecological spaces such as green spaces, water areas, and forest land are classified as carbon-absorbing land, and the carbon effects are negative [48].

At the district and block scales, except for ISL, the energy consumption of other carbon source land, such as RL and CL, mainly includes buildings, transportation, and waste treatment. Among them, the energy consumption of buildings accounts for more than 90%, including electricity, water, natural gas, etc., mainly used for heating, cooling, lighting, and equipment operation of buildings [49]. Studies show that electricity consumption and natural gas consumption are the main sources of carbon emissions from buildings. Among them, electricity consumption accounts for over 90%, while the carbon emissions from natural gas are generally within 1%, and some commercial and office buildings do not even consume natural gas [50]. Moreover, different types of UCLCE show a periodic change trend with the seasons, but it is consistent among different years, generally showing an increasing change trend. This study randomly selected the electricity consumption data of seven relatively mature blocks in a certain year by month and compared them with the total electricity consumption of each year for three consecutive years. The results further confirmed the above viewpoint (Figure 7). Therefore, this interannual increasing variation makes the UCLCE relatively stable within a certain period and also lays the foundation for subsequent predictions.

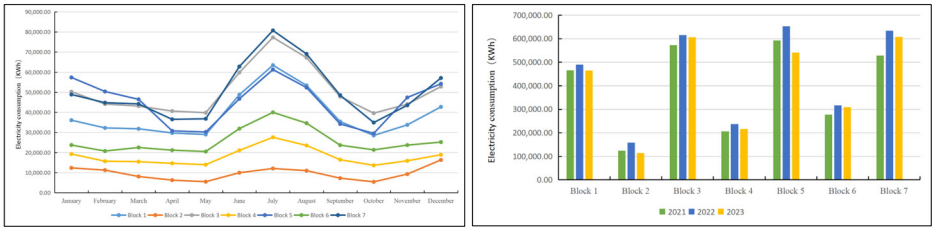


Figure 7. Comparison of monthly and annual electricity consumption of different blocks.

4.1.2. Prediction Mechanism: BEF Impact Effect

The UCLCE stems from the interaction between the BEF and energy consumption activities [51]. On one hand, the energy demand of UCL is affected by the user's perception of environmental comfort. The quality of the BEF directly determines the absorption or reflection of solar radiation by the building surface and the resulting heat exchange, which in turn changes the microclimate and affects energy consumption behavior [52]. For example, BEF such as density and morphology affect physical properties like temperature, humidity, lighting, and air flow, prompting building users to rely on artificial lighting, air conditioning, or heating equipment to regulate biological comfort, thereby increasing energy consumption [53]. On the other hand, the BEF affects the spatial distribution of UCLCE in its own unique way. Different types of UCL carry different building functions [54]. Buildings with different functions have different terminal energy consumption demands based on the content and intensity of activities of the users, which in turn affects the spatial agglomeration or dispersion characteristics of carbon effects [1]. The agglomeration effect of carbon emissions will further prompt government management departments to guide and shape a new BEF through urban planning means such as urban renewal, presenting a circular adaptation mechanism of "BEF–energy consumption activities–carbon effects–BEF" (Figure 8). Therefore, by constructing the logical relationship between the UCLCE and the BEF, it becomes the basis for the scientific prediction of the UCLCE.

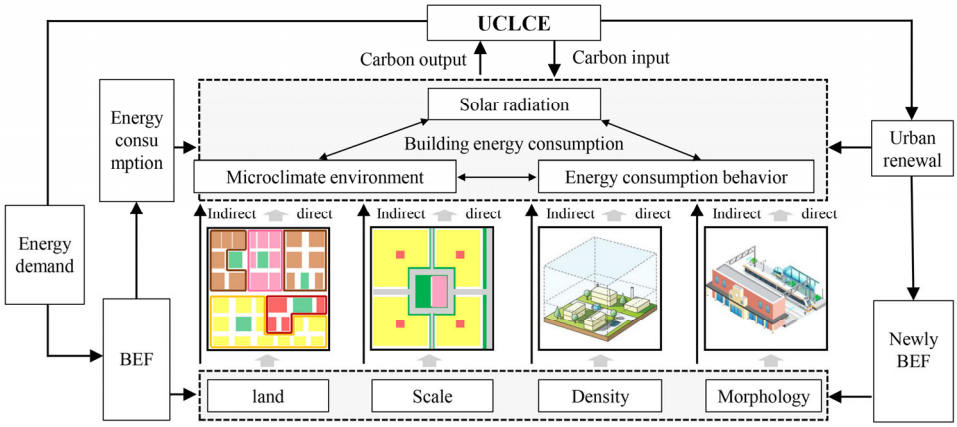


Figure 8. The influence mechanism of the BEF and the UCLCE.

4.2. Applications

To verify the applicability of this method in the prediction of carbon effects in urban planning schemes, the urban design scheme of the Taihu New Town area in Changxing was taken as an example for UCLCE prediction. Firstly, referring to the BEF of the current UCL in the central urban area, a database of BEF for planned UCL should be established. Secondly, based on the model establishment process proposed in the previous text, the UCLCE prediction results and spatial distribution of the planning scheme were obtained (Figure 9).

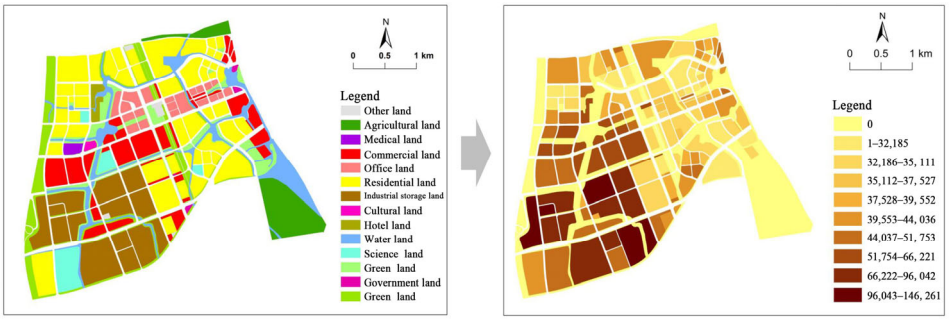


Figure 9. The carbon effect of the planning scheme.

Additionally, for the high-carbon effect blocks in the planning scheme, targeted low-carbon optimization methods for the BEF are proposed. By re-predicting the optimized urban planning scheme and comparing it with the UCLCE prediction results of the urban planning scheme before optimization, the carbon reduction benefits of the low-carbon optimization of the planning scheme can be accurately evaluated. The study selects two blocks, A and B, in the planning scheme as examples for detailed explanation (Figure 10). Before optimization, the carbon emissions of block A were 4.40×10^5 $kgCO_2$, and those of block B were 2.54×10^5 $kgCO_2$. After optimization, the carbon emissions of blocks $A-1$, $A-2$, $A-3$, and $A-4$ were 3.28×10^5 $kgCO_2$. A reduction of 1.12×10^5 $kgCO_2$, accounting for 25.45% of the carbon emissions of block A before optimization. The carbon emissions of block B after optimization are 2.42×10^5 $kgCO_2$. A reduction of 1.20×10^4 $kgCO_2$, accounting for 4.72% of the carbon emissions of block B before optimization. Therefore, the comparative analysis provides a scientific data basis and methodological support for the low-carbon optimization strategies of the BEF at the micro scale in quantitative analysis.

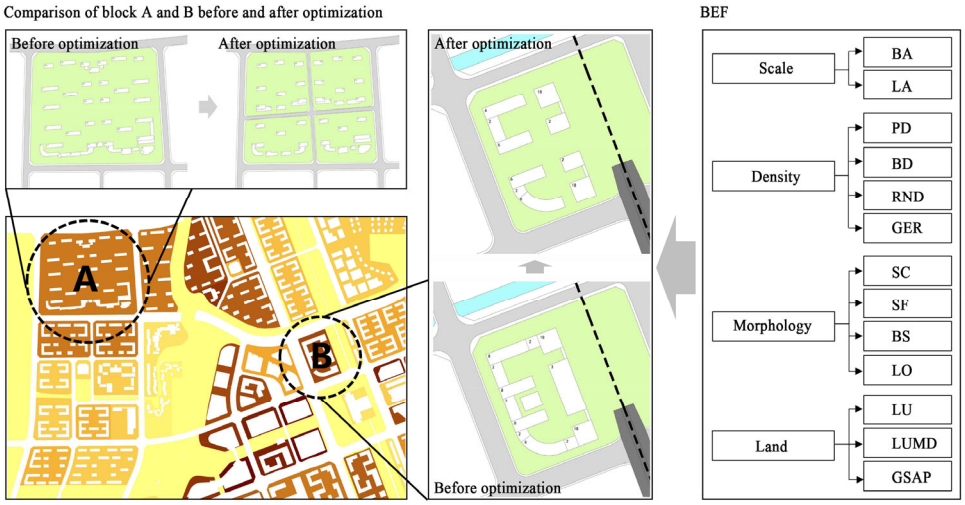


Figure 10. Comparison of carbon effects before and after the optimization of the BEF.

4.3. Limitations and Further Improvements

4.3.1. Applicability and Limitations

Centered on UCL with well-defined geographical boundaries, this study addresses the critical issue of poor compatibility between the carbon emissions accounting results of existing grid units and medium-to-micro scale spatial planning. Breaking through the limitations of traditional research, it offers a novel solution to integrate carbon accounting with spatial planning at finer scales. Insufficient systematic and dynamic consideration of UCLCE in existing studies is also addressed. By employing BEF such as scale, density, morphology, and land, this study simulates and predicts the carbon effect coefficients of different UCL types, thereby significantly enhancing the accuracy of UCLCE predictions.

However, the application of any model has certain applicability and limitations, especially when extended to other cities with different geographical and socio-economic conditions. First of all, it is applicability. On one hand, Changxing is situated in a hot summer and cold winter climate zone. This raises questions about the model's suitability for regions with fundamentally different climatic conditions. For example, temperate zones require significant winter heating alongside moderate summer cooling, while tropical zones demand intensive year-round cooling. Applying the model directly to such areas may therefore yield biased predictions. On the other hand, the case study benefited from comprehensive data, including a detailed 3D building vector database and smart electricity meter coverage exceeding 90%. In regions with less advanced data collection and management infrastructure, acquiring the necessary high-quality input data presents considerable challenges, potentially constraining the model's applicability. The second is the limitation.

Changxing is dominated by industrial and residential land, so the model is likely applicable to other cities with similar land use proportions. But for areas with primarily agricultural or ecological land use, the model may need retraining or input variable adjustments. Additionally, the model might struggle with special land use types like large sports venues or industrial park facilities, as their unique energy usage patterns aren't fully captured by the existing BEF. Furthermore, the model faces challenges in regions with rapid urban expansion or sharp land use changes. Since the model's training data is based on current land use and BEF characteristics, it may not accurately predict carbon emissions if a region undergoes rapid changes in the future.

4.3.2. Further Improvements

In future work, we aim to establish a more comprehensive method for measuring different types of UCLCE and develop a systematic data collection method to enhance the accuracy

and scientific validity of the prediction results. Firstly, the scope of data collection can be further expanded to incorporate more key variables that affect the UCLCE in the future. By collecting more comprehensive data, the model can depict the complex mechanism of UCLCE more accurately, thereby improving the prediction accuracy. Secondly, more rigorous cleaning and verification should be carried out on the existing multi-source data, and data mining techniques should be utilized to identify and correct outliers and error records. By establishing a data cross-validation mechanism, consistency checks are conducted on data from different sources. Thirdly, update the data regularly to reflect the dynamic changes in the carbon effect of urban construction land. Fourth, further adjust and optimize the model parameters, including appropriately increasing the number of hidden layers or neurons in the BP neural network, attempting to use different activation functions, adopting techniques such as L1, L2 regularization, or Dropout to prevent model overfitting, and adjusting the learning rate, etc. Finally, the BP neural network is multi-model fused with other machine learning models (such as support vector machine, random forest, etc.) to utilize the complementary advantages of different models and improve the accuracy and stability of prediction.

5. Conclusions

Taking the blocks of different types of UCL within the urban space as the basic research units, this study integrates the classification idea into the BP neural network model, proposes a prediction method for the UCLCE from the perspective of the BEF, and conducts an empirical study taking the central urban area of Changxing County, Zhejiang Province as an example. The results show that the BP neural network model has a good prediction effect on the carbon effect of different types of construction land, with an average error rate of 30.10%.

(1) The total effect and the intensity effect show significantly different changing trends. The total effect reflects the dynamic changes of the total carbon emissions from construction land, presenting a changing trend of ISL-OL-ML-L-SEL-CL-AL. The intensity effect reflects the fluctuation of carbon emission intensity per unit of construction land area, manifested as a downward trend of ISL-ML-CL-OL-RL-AL-SEL. The difference between the two provides a basis for a deeper understanding of the internal mechanism of UCLCE.

(2) The spatial distribution characteristics of carbon effects in UCL show a "⌟" spatial layout pattern, with significant positive spatial correlation, and Moran's I was 0.11. This means that spatially, the carbon effects of adjacent blocks are similar. Blocks with high carbon effects tend to be clustered and distributed, and vice versa for blocks with low carbon effects.

(3) By accurately identifying typical high-carbon effects blocks in the planning scheme and implementing targeted low-carbon optimization strategies, a carbon reduction benefit of 25.45% can be achieved, providing a practical and feasible path for the low-carbon development of towns.

This study offers significant insights into low-carbon planning strategies. Civic leaders can leverage predictive methods to evaluate the carbon impact of each urban block, thereby laying the groundwork for innovative carbon reduction initiatives. Meanwhile, urban planners can utilize these findings to optimize spatial organization, fostering a sustainable, low-carbon, and healthy trajectory for urban development.

Author Contributions: Conceptualization, Q.L., X.Z., Z.C. and X.Y.; data curation, X.Z. and Z.C.; formal analysis, Q.L., Z.C. and X.Y.; funding acquisition, X.Z. and Q.L.; investigation, Q.L. and X.Z.; methodology, Z.C., X.Z. and X.Y.; project administration, Q.L. and Z.C.; resources, X.Z. and X.Y.; software, Q.L. and Z.C.; supervision, Q.L. and X.Z.; validation, Z.C.; visualization, Q.L. and X.Z.; writing—original draft, Q.L. and X.Z.; writing—review and editing, Q.L. and X.Z. All authors have read and agreed to the published version of the manuscript.

Funding: This research was funded by the Humanities and Social Sciences Research Youth Fund Project of the Ministry of Education, grant no. 23YJCZH306, the Anhui Province University Science and Engineering Teachers' Internship Program in Enterprises, grant no. 2024JSQYGZ102, the Youth Fund of Shandong Natural Science Foundation, grant no. ZR2022QE151, and the Jinan Philosophy Social Science Project, grant no. JNSK2025B031.

Data Availability Statement: All data underlying the results are available as part of the article, and no additional source data are required.

Conflicts of Interest: Author Xunxi Yin is employed by the Zibo Urban Planning Design Institute Co., Ltd. The remaining authors declare that the research was conducted in the absence of any commercial or financial relationships that could be construed as a potential conflict of interest.

Abbreviations

Full Name	Abbreviation
Urban Construction Land	UCL
Built Environment Elements	BEF
Ordinary Least Square	OLS
Urban Residential Land	URL
Business Office Land	BOL
Medical Land	ML
Hotel Land	HL
Administrative Office Land	AOL
Other Land	OL
Building Area	BA
Population Density	PD
Road Network Density	RND
Spatial Compactness	SC
Building Story	BS
Land Use	LU
Green Space Area Proportion	GSAP
Administrative Land	AL
Urban Construction Land Carbon Effects	UCLCE
Support Vector Machine	SVM
Village Residential Land	VRL
Industrial Storage Land	ISL
Cultural and Sports Land	CSL
Commercial Land	CL
Science and Education Land	SEL
Green Space Land	GSL
Point of Interest	POI
Land Area	LA
Building Density	BD
Green Space Ratio	GSR
Shape Factor	SF
Land Orientation	LO
Land Use Mixing Degree	LUMD
Residential Land	RL

References

1. Xu, Y.; Sun, L.; Wang, B.; Ding, S.M.; Ge, X.C.; Cai, S.R. Research on the Impact of Carbon Emissions and Spatial Form of Town Construction Land: A Study of Macheng, China. *Land* **2023**, *12*, 1385. [CrossRef]
2. Zhang, X.P.; Liao, Q.H.; Yin, X.X.; Yin, Z.W.; Cao, Q.Q. Spatial Characteristics and Influencing Factors of Multi-Scale Urban Living Space (ULS) Carbon Emissions in Tianjin, China. *Buildings* **2023**, *13*, 2393. [CrossRef]

3. Zhang, X.P.; Liao, Q.H.; Zhao, H.; Li, P. Vector maps and spatial autocorrelation of carbon emissions at land patch level based on multi-source data. *Front. Public Health* **2022**, *10*, 1006337. [CrossRef] [PubMed]
4. Ou, Y.; Bao, Z.; Ng, S.T.; Song, W.; Chen, K. Land-use carbon emissions and built environment characteristics: A city-level quantitative analysis in emerging economies. *Land Use Policy* **2024**, *137*, 107019. [CrossRef]
5. Liu, G.; Cui, F.; Wang, Y. Spatial effects of urbanization, ecological construction and their interaction on land use carbon emissions/absorption: Evidence from China. *Ecol. Indic.* **2024**, *160*, 111817. [CrossRef]
6. Pu, J.; Xia, F. Exploring the relationship between city size and carbon emissions: An integrated population-land framework. *Appl. Geogr.* **2025**, *177*, 103571. [CrossRef]
7. Zhang, X.; Zhang, D. Urban carbon emission scenario prediction and multi-objective land use optimization strategy under carbon emission constraints. *J. Clean. Prod.* **2023**, *430*, 139684. [CrossRef]
8. Li, Y.; Peng, Y.-L.; Cheng, W.-Y.; Peng, H.-N. Spatial-temporal evolution and multi-scenario prediction of carbon emissions from land use in the adjacent areas of nature reserves. *Ecol. Indic.* **2025**, *170*, 113047. [CrossRef]
9. Li, X.K.; Zhang, C.R.; Li, W.D.; Anyah, R.O.; Tian, J. Exploring the trend, prediction and driving forces of aerosols using satellite and ground data, and implications for climate change mitigation. *J. Clean. Prod.* **2019**, *223*, 238–251. [CrossRef]
10. Qu, Y.; Zhan, L.; Zhang, Q.; Si, H.; Jiang, G. Towards sustainability: The impact of the multidimensional morphological evolution of urban land on carbon emissions. *J. Clean. Prod.* **2023**, *424*, 138888. [CrossRef]
11. Svirejeva-Hopkins, A.; Schellnhuber, H.J. Urban expansion and its contribution to the regional carbon emissions: Using the model based on the population density distribution. *Ecol. Model.* **2008**, *216*, 208–216. [CrossRef]
12. Chang, Y.; Xue, Y.; Song, S.; Geng, G. Analysis on carbon emission and peak forecasting of urban industrial zone renewal process in China based on extended Kaya identity. *Energy* **2025**, *315*, 134438. [CrossRef]
13. Yang, Y.; Yang, M.; Zhao, B.; Lu, Z.; Sun, X.; Zhang, Z. Spatially explicit carbon emissions from land use change: Dynamics and scenario simulation in the Beijing-Tianjin-Hebei urban agglomeration. *Land Use Policy* **2025**, *150*, 107473. [CrossRef]
14. Chuai, X.; Feng, J. High resolution carbon emissions simulation and spatial heterogeneity analysis based on big data in Nanjing City, China. *Sci. Total Environ.* **2019**, *686*, 828–837. [CrossRef]
15. Lin, F.-Y.; Lin, T.-P.; Hwang, R.-L. Using geospatial information and building energy simulation to construct urban residential energy use map with high resolution for Taiwan cities. *Energy Build.* **2017**, *157*, 166–175. [CrossRef]
16. Zhang, X.; Xie, Y.; Jiao, J.; Zhu, W.; Guo, Z.; Cao, X.; Liu, J.; Xi, G.; Wei, W. How to accurately assess the spatial distribution of energy CO_2 emissions? Based on POI and NPP-VIIRS comparison. *J. Clean. Prod.* **2023**, *402*, 136656. [CrossRef]
17. Al-Kabaha, Y.; Bataineh, K.; Aburabi'e, M. Multi-objective optimization of energy consumption, cost and emission for a residential building. *Heliyon* **2025**, *11*, e42139. [CrossRef]
18. Eid, E.; Foster, A.; Alvarez, G.; Ndoye, F.-T.; Leducq, D.; Evans, J. Modelling energy consumption in a Paris supermarket to reduce energy use and greenhouse gas emissions using EnergyPlus. *Int. J. Refrig.* **2024**, *168*, 1–8. [CrossRef]
19. Bahadori, E.; Rezaei, F.; He, B.-J.; Heiranipour, M.; Attia, S. Evaluating urban heat island mitigation strategies through coupled UHI and building energy modeling. *Build. Environ.* **2025**, *280*, 113111. [CrossRef]
20. Zhang, L.; Sang, G.; Cui, X.; Han, W. Design optimization of rural building in dry-hot and dry-cold area using a back propagation (BP) neural network. *Energy Build.* **2022**, *259*, 111899. [CrossRef]
21. Lei, R.; Yin, J. Prediction method of energy consumption for high building based on LMBP neural network. *Energy Rep.* **2022**, *8*, 1236–1248. [CrossRef]
22. Zhang, L.; Sang, G.C.; Han, W.X. Effect of hygrothermal behaviour of earth brick on indoor environment in a desert climate. *Sust. Cities Soc.* **2020**, *55*, 102070. [CrossRef]
23. Li, Q.D.; Sun, X.; Chen, C.; Yang, X.D. Characterizing the household energy consumption in heritage Nanjing Tulou buildings, China: A comparative field survey study. *Energy Build.* **2012**, *49*, 317–326. [CrossRef]
24. Zhao, L.; Zhang, C.; Wang, Q.; Yang, C.; Zhou, W. Spatio-temporal variations of land use carbon emissions and its low carbon strategies for coastal areas in China with nighttime lighting data. *J. Environ. Manag.* **2025**, *385*, 125651. [CrossRef]
25. Du, L.; Peng, C.; Ren, H.; Wu, Z.; Gao, W. Assessing Annual Carbon Emissions and its Peak Year in the Yangtze River Economic Belt (2021–2035) through Land Use/Land Cover Analysis. *Sust. Cities Soc.* **2025**, *127*, 106453. [CrossRef]
26. Xu, C.G.; Xiong, W.; Zhang, S.M.; Shi, H.L.; Wu, S.C.; Bao, S.J.; Xiao, T.Q. Research on the Nonlinear Relationship Between Carbon Emissions from Residential Land and the Built Environment: A Case Study of Susong County, Anhui Province Using the XGBoost-SHAP Model. *Land* **2025**, *14*, 440. [CrossRef]
27. Yu, Z.; Chen, L.; Tong, H.; Chen, L.; Zhang, T.; Li, L.; Yuan, L.; Xiao, J.; Wu, R.; Bai, L.; et al. Spatial correlations of land-use carbon emissions in the Yangtze River Delta region: A perspective from social network analysis. *Ecol. Indic.* **2022**, *142*, 109147. [CrossRef]
28. Das, M.; Das, A. Dynamicity of carbon emission and its relationship with heat extreme and green spaces in a global south tropical mega-city region. *Atmos. Pollut. Res.* **2025**, *16*, 102484. [CrossRef]
29. Wang, X.P.; Li, Z.Y.; Kee, T. Spatial and temporal correlation between green space landscape pattern and carbon emission-Three major coastal urban agglomerations in China. *Urban Clim.* **2024**, *58*, 102222. [CrossRef]

30. Bai, J.; Chen, H.; Gu, X.; Ji, Y.; Zhu, X. Temporal and spatial characteristics of carbon emissions from cultivated land use and their influencing factors: A case study of the Yangtze River Delta region. *Int. Rev. Econ. Financ.* **2024**, *96*, 103501. [CrossRef]
31. Zhao, Q.Y.; Xie, B.Y.; Han, M.Y. Unpacking the Sub-Regional Spatial Network of Land-Use Carbon Emissions: The Case of Sichuan Province in China. *Land* **2023**, *12*, 1927. [CrossRef]
32. Luo, Z.X.; Yang, L.; Liu, J.P. Embodied carbon emissions of office building: A case study of China's 78 office buildings. *Build. Environ.* **2016**, *95*, 365–371. [CrossRef]
33. Wang, L.; Chen, T.; Yu, Y.; Wang, L.Y.; Zang, H.Y.; Cang, Y.; Zhang, Y.O.; Ma, X.W. Impacts of Vegetation Ratio, Street Orientation, and Aspect Ratio on Thermal Comfort and Building Carbon Emissions in Cold Zones: A Case Study of Tianjin. *Land* **2024**, *13*, 1275. [CrossRef]
34. Wang, L. Assessment of land use change and carbon emission: A Log Mean Divisa (LMDI) approach. *Heliyon* **2024**, *10*, e25669. [CrossRef] [PubMed]
35. Shi, Y.S.; Zheng, B.; Wang, Z.; Zheng, J.W. Mixed Land Use and Its Relationship with CO_2 Emissions: A Comparative Analysis Based on Several Typical Development Zones in Shanghai. *Land* **2023**, *12*, 1675. [CrossRef]
36. Ji, R.R.; Wang, K.; Zhou, M.R.; Zhang, Y.; Bai, Y.J.; Wu, X.; Yan, H.; Zhao, Z.Q.; Ye, H. Green Space Compactness and Configuration to Reduce Carbon Emissions from Energy Use in Buildings. *Remote Sens.* **2023**, *15*, 1502. [CrossRef]
37. Luo, H.; Zhang, Y.; Gao, X.; Liu, Z.; Song, X.; Meng, X.; Yang, X. Unveiling land use-carbon Nexus: Spatial matrix-enhanced neural network for predicting commercial and residential carbon emissions. *Energy* **2024**, *305*, 131722. [CrossRef]
38. Zhang, M.; Kafy, A.A.; Xiao, P.; Han, S.; Zou, S.; Saha, M.; Zhang, C.; Tan, S. Impact of urban expansion on land surface temperature and carbon emissions using machine learning algorithms in Wuhan, China. *Urban Clim.* **2023**, *47*, 101347. [CrossRef]
39. Tian, D.; Zhang, J.; Li, B.; Xia, C.; Zhu, Y.; Zhou, C.; Wang, Y.; Liu, X.; Yang, M. Spatial analysis of commuting carbon emissions in main urban area of Beijing: A GPS trajectory-based approach. *Ecol. Indic.* **2024**, *159*, 111610. [CrossRef]
40. Zhou, Y.; Hu, D.; Wang, T.; Tian, H.; Gan, L. Decoupling effect and spatial-temporal characteristics of carbon emissions from construction industry in China. *J. Clean. Prod.* **2023**, *419*, 138243. [CrossRef]
41. Freitas, W.W.L.; de Souza, R.M.C.R.; Amaral, G.J.A.; Bastiani, F.D. Exploratory spatial analysis for interval data: A new autocorrelation index with COVID-19 and rent price applications. *Expert Syst. Appl.* **2022**, *195*, 116561. [CrossRef]
42. Mtshawu, B.; Bezuidenhout, J.; Kilel, K.K. Spatial autocorrelation and hotspot analysis of natural radionuclides to study sediment transport. *J. Environ. Radioact.* **2023**, *264*, 107207. [CrossRef]
43. Gedamu, W.T.; Plank-Wiedenbeck, U.; Wodajo, B.T. A spatial autocorrelation analysis of road traffic crash by severity using Moran's I spatial statistics: A comparative study of Addis Ababa and Berlin cities. *Accid. Anal. Prev.* **2024**, *200*, 107535. [CrossRef]
44. Li, W.Y.; Wang, K.Q.; Liu, H.M.; Zhang, Y.X.; Zhu, X.D. Construction Land Transfer Scale and Carbon Emission Intensity: Empirical Evidence Based on County-Level Land Transactions in Jiangsu Province, China. *Land* **2024**, *13*, 917. [CrossRef]
45. Fang, Y.; Zhao, L. Exploring the decoupling effect and driving mechanism of carbon emissions at macroscale: An empirical study from Wuhan metropolitan area. *Urban Clim.* **2025**, *61*, 102434. [CrossRef]
46. Lin, Q.W.; Zhang, L.; Qiu, B.K.; Zhao, Y.; Wei, C. Spatiotemporal Analysis of Land Use Patterns on Carbon Emissions in China. *Land* **2021**, *10*, 141. [CrossRef]
47. Wu, Z.H.; Zhou, L.H.; Wang, Y.B. Prediction of the Spatial Pattern of Carbon Emissions Based on Simulation of Land Use Change under Different Scenarios. *Land* **2022**, *11*, 1788. [CrossRef]
48. Wang, C.; Yang, Y.J.; Bai, Y.P.; Teng, Y.M.; Zhan, J.Y. Land use data can improve the accuracy of carbon emission spatial inversion model. *Land Degrad. Dev.* **2024**, *35*, 2345–2366. [CrossRef]
49. Li, Z.; Sun, H.; Long, J.; Qiu, S. Study on the matching characteristics between office building energy consumption and rooftop photovoltaics in regions with hot summers and cold winters. *Renew. Energy* **2025**, *249*, 123285. [CrossRef]
50. Kaloop, M.R.; Ahmad, F.; Samui, P.; Elbeltagi, E.; Hu, J.-W.; Wefki, H. Predicting energy consumption of residential buildings using metaheuristic-optimized artificial neural network technique in early design stage. *Build. Environ.* **2025**, *274*, 112749. [CrossRef]
51. Delmastro, C.; Mutani, G.; Pastorelli, M.; Vicentini, G. Urban morphology and energy consumption in Italian residential buildings. In Proceedings of the 2015 International Conference on Renewable Energy Research and Applications (ICRERA), Palermo, Italy, 22–25 November 2015.
52. Li, Z.W.; Dai, J.; Chen, H.Z.; Lin, B.R. An ANN-based fast building energy consumption prediction method for complex architectural form at the early design stage. *Build. Simul.* **2019**, *12*, 665–681. [CrossRef]
53. Wang, P.; Yang, Y.T.; Ji, C.; Huang, L. Positivity and difference of influence of built environment around urban park on building energy consumption. *Sust. Cities Soc.* **2023**, *89*, 104321. [CrossRef]
54. Dujardin, S.; Marique, A.F.; Teller, J. Spatial planning as a driver of change in mobility and residential energy consumption. *Energy Build.* **2014**, *68*, 779–785. [CrossRef]

Disclaimer/Publisher's Note: The statements, opinions and data contained in all publications are solely those of the individual author(s) and contributor(s) and not of MDPI and/or the editor(s). MDPI and/or the editor(s) disclaim responsibility for any injury to people or property resulting from any ideas, methods, instructions or products referred to in the content.